



CHORUS

This is the accepted manuscript made available via CHORUS. The article has been published as:

Vibrational spectra and nonlinear optical coefficients of rhombohedral CsGeX_3 halide compounds with $X=\text{I, Br, Cl}$

Ling-yi Huang and Walter R. L. Lambrecht

Phys. Rev. B **94**, 115202 — Published 12 September 2016

DOI: [10.1103/PhysRevB.94.115202](https://doi.org/10.1103/PhysRevB.94.115202)

Vibrational spectra and non-linear optical coefficients of rhombohedral CsGeX₃ halide compounds with X=I, Br, Cl.

Ling-yi Huang and Walter R. L. Lambrecht*

Department of Physics, Case Western Reserve University, Cleveland, OH 44106-7079

The zone-center phonons are calculated for rhombohedral CsGeX₃ compounds with X=I, Br, Cl using density functional perturbation theory in a plane-wave pseudopotential method. The infrared absorption and reflection spectra are simulated and show that the absorption has a strong contribution from the LO as well as TO modes. Both the lowest and highest IR active modes have strong oscillator strengths for each symmetry (A_1 and E) and correspond to motions of either the Cs or Ge ions relative to the halogen ions respectively. The intermediate modes have low oscillator strength because their mode pattern shows less clearly a dipole pattern. The polarization dependent Raman spectra for various back-scattering configurations are simulated. Only the highest modes of each symmetry have a strong Raman intensity. The results for the Raman spectra are found to be in good agreement with the available experimental data for polycrystalline films when averaging over directions. The Born effective charges and high and low frequency dielectric tensors as well as the second-order nonlinear optical coefficients are calculated. The ratio of the static to the high-frequency dielectric constants are extremely high and analyzed in terms of the contribution of each mode to the Lyddane-Sachs-Teller relation. The non-linear optical coefficients decrease strongly from I to Br to Cl in reverse order of the band gaps and are found to be consistent with available experimental results.

I. INTRODUCTION

The halide perovskites ABX₃ with X a halogen, B a group four element (Pb,Sn,Ge) and A either Cs or an organic radical such as methylammonium (MA) are currently under intense investigation as materials for solar cells,¹⁻³ field effect transistors,⁴ and non-linear optical materials.⁵ Although mainly (MA)PbI₃ has received attention as highly efficient solar cell material, other members of this family are of interest as well. In a recent paper,⁶ we pointed out the potential advantages of the much less studied Ge based compounds in this family. First CsGeI₃ also has a suitable band gaps for photovoltaics ($E_g = 1.6$ eV in the rhombohedral and 1.20 eV in the cubic structure) and secondly these materials distort from the ideal cubic perovskite structure in a different way from the Pb and Sn based compounds. This is related to the tolerance factor in the perovskite structure $t = (R_A + R_C)/\sqrt{2}(R_B + R_C)$ where R_A , R_B , R_C are the ionic radii. While this factor is less than 1 in the Sn and Pb cases, it is larger than 1 for Ge. A tolerance factor $t < 1$ indicates that the open space in the network of the corner-sharing octahedra is too large for the A atom or molecular radical occupying that site. This indicates that the structure will try to become denser first by rotating the octahedra about various tilt axes^{7,8} and secondly by possible instabilities to an edge-sharing octahedral structure.⁹ The latter is detrimental for solar cells as it has a much higher band gap, unsuitable for photovoltaics. On the other hand in the Ge compounds, which have $t > 1$, this instability does not occur. However, another instability of the cubic perovskite occurs, namely a ferro-electric instability, where the Ge moves off the center site along the [111] direction of the cubic structure. This is then accompanied by a rhombohedral distortion of the lattice vectors leading to a $R3m$ space-

group C_{3v}^5 .¹⁰ As was shown in Ref.6 this leads to a rather mild distortion of the band structure which has only a slightly larger gap than the cubic structure.

Clearly because of these various structural instabilities of the perovskite structure, the vibrational properties are quite important. Although Raman spectra have been reported for some of the CsGeX₃ compounds,^{5,11,12} the current understanding of the phonon spectra is rather incomplete. In the present paper we focus on the vibrational spectra of rhombohedral CsGeX₃ and present a first-principles calculation of the zone-center phonons and the associated Raman and infrared spectra.

The rhombohedral ferro-electrically distorted structure has no inversion symmetry and thus the CsGeX₃ compounds have also been considered for second-order nonlinear optical (NLO) applications.^{5,13} Their birefringence may also allow for phase-matching. Here not only CsGeI₃ but also the wider gap Br and Cl compounds are of interest. In the low-frequency limit, the second order nonlinear optical coefficients can be calculated by the density functional perturbation theory (DFPT) in a similar manner as the force constants, Born effective charges and Raman tensor components. All are either second or third or mixed derivatives of the total energy versus atomic displacements and static electric fields.

After briefly describing the methodology used, we proceed to analyze the phonon frequencies, Raman and infrared spectra, including a discussion of the experimental data available to date, the Born charges, dielectric constants and non-linear optical coefficients. The present work follows up on our earlier study of lattice dynamics in Sn based halide perovskites but has no overlap with that paper.⁸

II. METHODS

We use the density functional perturbation theory,^{14,15} which is equivalent to linear response theory,^{16,17} to calculate the phonons as implemented in a plane-wave pseudopotential method in the ABINIT code.¹⁸ More specifically, we use Hartwigsen-Goedecker-Hutter (HGH) pseudo-potentials,¹⁹ and an energy cut-off of 60 Hartrees, which was found to be well converged by initial tests. In these pseudopotentials only the outer valence s and p electrons (4s,4p) for Ge, (3s,3p) for Cl, (4s,4p) for Br, (5s,5p) for I are treated as valence. For Cs, on the other hand, the 6s as well as the 5s and 5p semicore states are treated as valence. An $8 \times 8 \times 8$ shifted k-point mesh was used and also tested first for convergence. We use the local density approximation as parametrized by Perdew and Wang²⁰ which is based on the Ceperley-Alder calculations of the electron gas.²¹ This parametrization matches well the exchange-correlation parametrization by Goedecker-Teter-Hutter²² used in the generation of the pseudopotentials. Since the LDA tends to overestimate bond strengths it may also be expected to slightly overestimate phonon frequencies. Spin-orbit coupling effects are not included here since they are expected to be relatively less important for Ge based compounds and for integrated electronic quantities like force constants entering the phonon calculations. They could be more important for specific electronic structure aspects and were included in our previous study of the band structures.⁶

The Raman tensors and Raman intensities are calculated following the method described in Veithen *et al.*²³. The eigenvectors of the phonon calculations along with the Born effective charges straightforwardly provide the oscillator strengths from which one obtains the phonon contribution to the frequency dependent dielectric functions. These are then directly related to the infrared absorption and reflection spectra. The calculations were performed for the experimental lattice constants as given in Thiele *et al.*¹⁰.

III. RESULTS

A. Group theoretical considerations

The point group is C_{3v} which has as irreducible representations A_1 , A_2 , E . The A_1 irreducible representation corresponds to basis functions z , $x^2 + y^2$, or z^2 . The irreducible representation E is doubly degenerate and corresponds to basis function pairs (x, y) , $(2xy, x^2 - y^2)$, (xz, yz) . The A_2 irrep corresponds to a rotation about the z -axis R_z . The 5 atoms in the unit cell give rise to 3 A_1 modes and 4 E modes which are optically active in infrared, A_1 for polarization along z and E for polarization along x or y or anywhere in the xy -plane. These modes are also all Raman active. There is one silent A_2 mode. Together with the zero-frequency acoustic mode of symmetry A_1 (corresponding to a uniform translation along

z) and the doubly degenerate E corresponding to translation in the xy -plane, this accounts for the 15 degrees of freedom. Here it is assumed that z is along the 3-fold symmetry axis of the structure. The Raman tensors for modes of A_1 symmetry has the form

$$\begin{pmatrix} a & & \\ & a & \\ & & b \end{pmatrix} \quad (1)$$

while the modes of E symmetry have the form

$$\begin{pmatrix} c & & \\ & -c & d \\ & & d \end{pmatrix} \quad \text{or} \quad \begin{pmatrix} & c & d \\ c & & \\ d & & \end{pmatrix}, \quad (2)$$

where the first matrix corresponds to $E(y)$ and the second to $E(x)$. Examples of different scattering geometries can be found at <http://www.cryst.ehu.es/cryst/polarizationselrules.html>. The scattering geometry is usually specified in terms of the Porto²⁴ notation $k_i(e_i e_s)k_s$ giving the incoming wave vector k_i , incoming polarization e_i , scattered wavevector k_s and polarization e_s . For example for backscattering geometry $-y(xx)y$ one would find both A_1 and E modes with the A_1 being TO modes and the E -modes LO modes and the intensity of the A_1 modes would be proportional to a^2 while that of the E_{LO} modes would be given by c^2 . It will thus suffice to give the values of a, b, c, d for TO and LO modes to allow one to reconstruct the spectra for various scattering configurations.

B. Mode frequencies and Raman spectra.

In table I we give the phonon frequencies, Raman tensor components and IR oscillator strengths for CsGeI₃, CsGeBr₃ and CsGeCl₃. One can clearly see that only the highest frequency A_1 and E modes have significant Raman intensity. The other modes have one to two orders of magnitude smaller Raman tensor components and the latter comes in squared in the Raman intensity.

In Figs. 1,2,3 we show the simulated Raman spectra for various back-scattering geometries for CsGeI₃, CsGeBr₃ and CsGeCl₃ respectively.

C. Infrared spectra

Simulated infrared spectra are given for each material in Fig. 4, 5 and 6. For each material, we show $\text{Im} \varepsilon(\omega)$, whose peaks correspond to the TO modes, $-\text{Im} \varepsilon^{-1}(\omega)$ whose peaks give the LO modes, $\text{Re} \varepsilon(\omega)$, the zeros of which also give the LO modes, as well as the infrared reflectivity $R = |(\tilde{n} - 1)/(\tilde{n} + 1)|^2$ with \tilde{n} the complex index of refraction $\tilde{n}^2 = \varepsilon$ and the absorption coefficient $\alpha(\omega) = 2\omega \text{Im} \varepsilon(\omega)/n(\omega)$ with $n(\omega) = \text{Re} \tilde{n}(\omega)$ the real part of the index of refraction. We can see that

TABLE I. Phonon frequencies (in cm^{-1}), and their Raman tensor components (in atomic units $\times 10^{-3}$) and IR oscillator strengths (S_α in atomic units $\times 10^{-5}$) for CsGeI_3 , CsGeBr_3 and CsGeCl_3 .

CsGeI ₃							
Symmetry	ω (cm^{-1})	ω (cm^{-1})	a-TO	Raman tensor components			IR S_z
	TO	LO		a-LO	b-TO	b-LO	
A_1	5.70	19.98	-0.57	-4.79	-0.31	-4.58	1.296
A_1	61.29	63.41	3.86	-0.30	3.36	-0.93	0.839
A_1	137.21	161.54	39.28	33.22	44.21	39.49	16.661
	TO	LO	c-TO	c-LO	d-TO	d-LO	$S_x = S_y$
E	19.24	26.05	-0.26	-4.13	-0.38	-6.68	1.384
E	31.78	31.95	-0.54	-1.64	0.14	-1.61	0.026
E	50.64	50.81	1.01	-0.16	0.91	-0.95	0.073
E	113.56	155.64	-31.29	26.09	-50.51	42.49	25.329
A_2	25.08						
CsGeBr ₃							
Symmetry	ω (cm^{-1})	ω (cm^{-1})	a-TO	Raman tensor components			IR S_z
	TO	LO		a-LO	b-TO	b-LO	
A_1	11.02	27.80	-0.48	-3.13	-0.32	-3.45	1.279
A_1	82.54	83.54	4.70	3.12	6.27	4.47	0.318
A_1	165.01	200.32	-22.22	19.69	-24.73	21.39	16.219
	TO	LO	c-TO	c-LO	d-TO	d-LO	$S_x = S_y$
E	22.52	30.87	-0.33	-2.47	-0.39	-3.85	1.243
E	41.71	42.80	0.28	-1.08	0.61	-1.54	0.159
E	67.00	67.57	1.62	0.49	2.79	0.99	0.192
E	135.56	188.63	-17.80	16.13	-27.95	24.80	21.514
A_2	32.40						
CsGeCl ₃							
Symmetry	ω (cm^{-1})	ω (cm^{-1})	a-TO	Raman tensor components			IR S_z
	TO	LO		a-LO	b-TO	b-LO	
A_1	13.53	40.57	-0.38	-1.53	-0.14	-1.54	1.519
A_1	134.03	134.54	3.75	4.26	3.94	4.49	0.144
A_1	249.04	293.92	-12.94	11.70	-13.72	11.38	17.537
	TO	LO	c-TO	c-LO	d-TO	d-LO	$S_x = S_y$
E	15.70	37.04	-0.20	-1.26	-0.26	-2.03	1.523
E	58.72	58.93	-0.30	-0.52	0.23	-0.13	0.022
E	106.04	106.16	0.79	1.01	0.68	1.03	0.035
E	207.53	273.37	-10.09	9.76	-15.27	14.05	23.706
A_2	40.60						

the lowest A_1 and E modes have unexpectedly large oscillator strength. Although it does not show up as a strong absorption band (because of the low ω factor), it should show up clearly in IR reflectivity. The highest modes which have also the largest Raman intensity are the strongest modes. It is also noteworthy that the in-

frared absorption does not only show peaks at the TO modes but also at the highest LO modes.

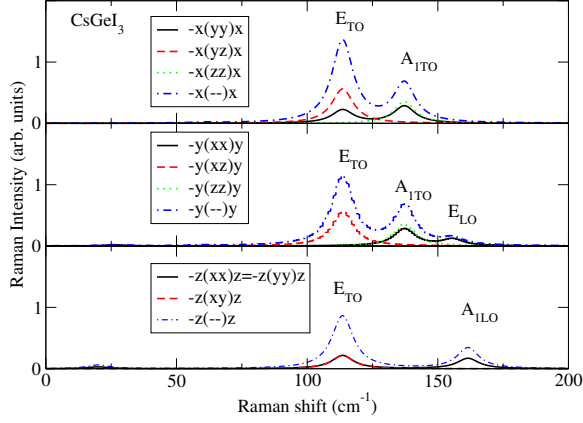


FIG. 1. (Color on-line) Simulated Raman spectra for CsGeI₃ in back-scattering geometries with beam along x , y , or z and various polarizations. $x(- -)x$ means no polarization and is the sum of $-x(yy)x$, $-x(yz)x$, $-x(zy)x$ and $-x(zz)x$.

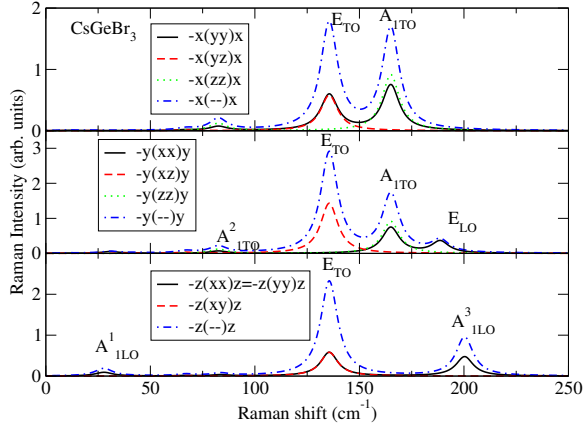


FIG. 2. (Color on-line) Simulated Raman spectra for CsGeBr₃ in back-scattering geometries with beam along x , y , or z and various polarizations. $x(- -)x$ means no polarization and is the sum of $-x(yy)x$, $-x(yz)x$, $-x(zy)x$ and $-x(zz)x$.

D. Discussion: comparison with experimental data.

For CsGeI₃, there are several Raman studies available. Tang *et al.*¹¹ found two main peaks in the Raman spectrum at $\omega_1 = 105 \text{ cm}^{-1}$ and $\omega_2 = 151 \text{ cm}^{-1}$. These were assigned to symmetric and antisymmetric stretching modes of the GeI₃ tetrahedron. No polarization selective analysis was presented. In addition they found smaller peaks which can be interpreted as overtones at $220 \text{ cm}^{-1} \approx 2\omega_1$, at $268 \text{ cm}^{-1} \approx \omega_1 + \omega_2$ and 293

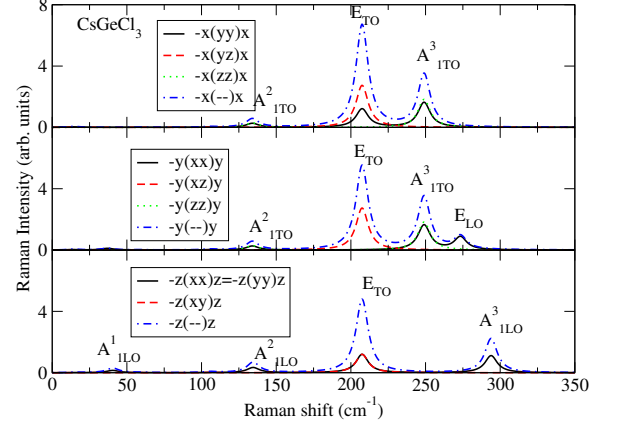


FIG. 3. (Color on-line) Simulated Raman spectra for CsGeCl₃ in back-scattering geometries with beam along x , y , or z and various polarizations. $x(- -)x$ means no polarization and is the sum of $-x(yy)x$, $-x(yz)x$, $-x(zy)x$ and $-x(zz)x$.

$\text{cm}^{-1} \approx 2\omega_2$. More recently Stoumpos *et al.*⁵ found also two rather broad peaks in the Raman spectrum of CsGeI₃ at 127 and 172 cm^{-1} . The results of Tang *et al.*¹¹ are fairly close to our calculated E_{TO} and E_{LO} modes at 113 cm^{-1} and 156 cm^{-1} and indicate that their scattering geometry may have favored the E -modes. Several of the right-angle scattering geometries, *e.g.* $x(yz)y$, $y(xx)z$, $y(xy)x$, etc. give E_{LO+TO} . The simulated spectra for back-scattering in Fig. 1 shows that for beams along x , or y three peaks would be seen, at E_{TO} , A_{1TO} and E_{LO} , but for the beam along z , one would see E_{1TO} and A_{1LO} . Since the A_{1LO} peak is only slightly higher than the E_{LO} peak at about 161 cm^{-1} , it could provide an alternative explanation for the Tang *et al.*'s¹¹ observed spectrum. It would indicate that both modes are slightly overestimated in our calculation. Unfortunately the authors of this paper did not report their scattering geometry. As for the Stoumpos *et al.* results⁵, the lowest peak at 127 cm^{-1} corresponds to an average of A_{1TO} and E_{TO} at 125 cm^{-1} . This could be expected for a polycrystalline sample with no preference for different orientations. However the corresponding average of the LO modes in our calculation is 159 cm^{-1} while the experiment gives 172 cm^{-1} . However, as we pointed out before for CsSnI₃,⁸ such a shift of the LO mode could well be explained by an LO-plasmon coupling effect if the samples are somewhat conductive. In fact, using

$$\omega_P^2 = \frac{4\pi n_h e^2}{\epsilon_\infty m_h}$$

we can estimate for which carrier concentration the plasmon frequency ω_P equals the LO-frequency. Using the low effective hole mass, $m_h = 0.087$ in CsGeI₃, obtained from the band structure calculations reported in Ref. 6,

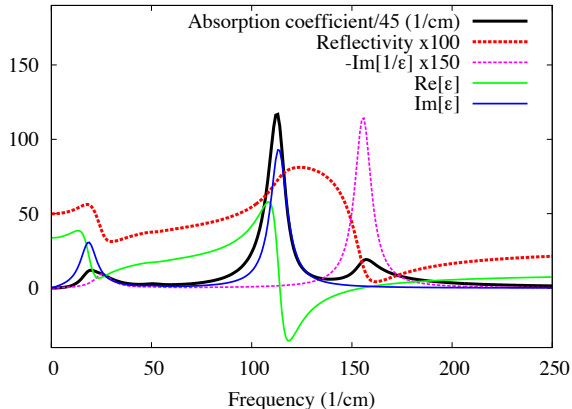
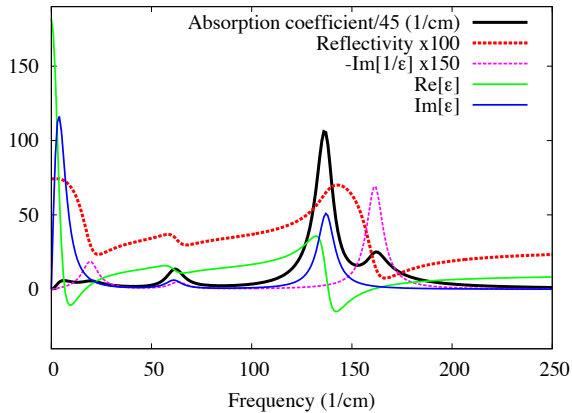


FIG. 4. (Color on-line) Infrared spectra for CsGeI₃ for A_1 -symmetry or $\mathbf{E} \parallel \mathbf{c}$ (top) and E -symmetry or $\mathbf{E} \perp \mathbf{c}$ (bottom).

the electronic dielectric constant $\epsilon_\infty = 9.63$ shows that an LO frequency of 19 meV or 160 cm^{-1} is reached for a hole concentration $n_h \approx 2 \times 10^{17} \text{ cm}^{-3}$. This is similar to hole concentrations previously reported in CsSnI₃. Thus it is likely that we are in a strong plasmon-coupling regime. In the LO-plasmon coupling regime, the upper branch becomes increasingly more plasmon like and increases with carrier concentration.

For CsGeBr₃ and CsGeCl₃, a more complete set of phonon modes were reported by Tang *et al.*¹¹ which we compare with our calculated modes we assign to them in Table II. More recently, Lin *et al.*¹³ studied mixed CsGe(Br_{*x*}Cl_{*1-x*})₃ crystals. The three highest frequency and also strongest Raman peaks for CsGeBr₃ and CsGeCl₃ were already reported by Thiele *et al.*¹⁰ These authors also mention that the highest peaks disappear above the phase transition to the cubic phase, which only shows two broad bands at 251, 204 cm^{-1} for the Cl compound and 162, 142 cm^{-1} for the Br compound. They conclude that this indicates an order-disorder transition since first-order Raman spectra are forbidden in the cubic structure. The overall agreement is quite good although not perfect. It should be kept in mind that the experimental work did not include a study of the polarization

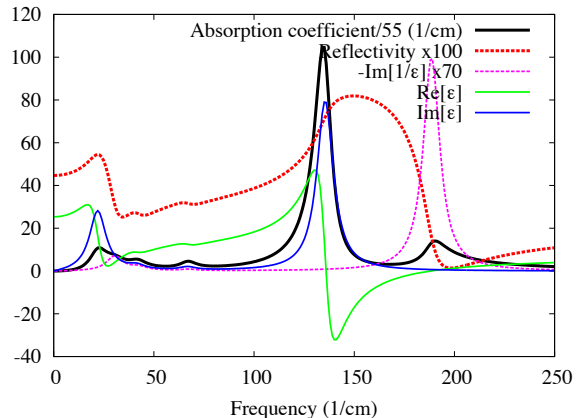
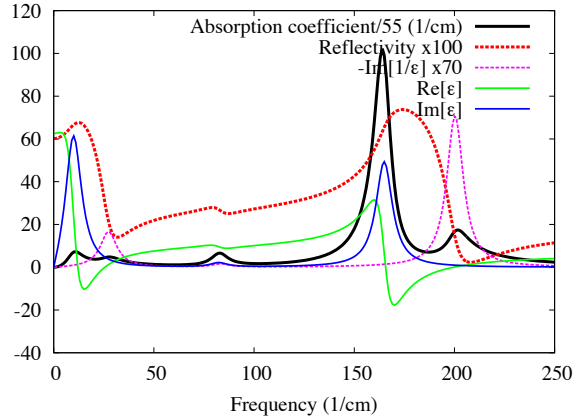


FIG. 5. (Color on-line) Infrared spectra for CsGeBr₃ for A_1 -symmetry or $\mathbf{E} \parallel \mathbf{c}$ (top) and E -symmetry or $\mathbf{E} \perp \mathbf{c}$ (bottom).

dependence or an analysis versus crystallographic directions, and thus our assignments are somewhat tentative.

We also show in Fig. 7 a simulated spectrum which is the superposition of the $x(\text{---})x$, $y(\text{---})y$, $z(\text{---})z$ spectra, so assuming any direction is equally likely and each one already averaged over polarizations and using a somewhat larger broadening factor. This spectrum looks quite closely like the experimental spectrum. Strictly speaking, one should actually integrate over angles and also the LO-TO splitting actually will vary with angle of the beam. So, this is still only an approximate way of averaging.

E. Mode-patterns

In figures 9 we show the vibrational patterns for a few vibrational modes. In Fig. 9a we show the lowest vibrational mode of A_1 symmetry. One can see that in this mode the Cs ions move opposite to the I ions with the largest displacement being for the Cs ions. Because of their opposite charges, this mode can be expected to have a fairly large oscillator strength, which is consistent with our findings for the IR spectra and Table I. In Fig. 9b we show the highest mode of A_1 symmetry.

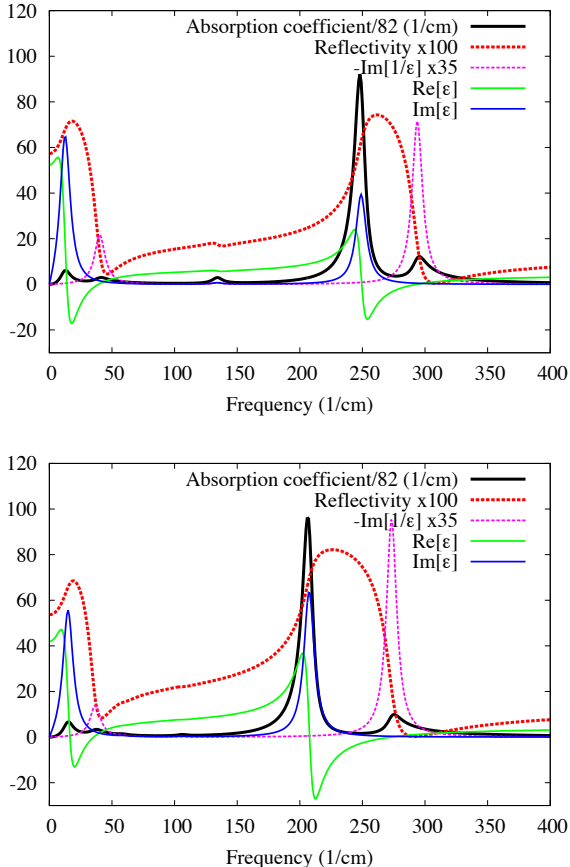


FIG. 6. (Color on-line) Infrared spectra for CsGeCl₃ for A₁-symmetry or $\mathbf{E} \parallel \mathbf{c}$ (top) and E-symmetry or $\mathbf{E} \perp \mathbf{c}$ (bottom).

Here the Ge is moving opposite to the I atoms and primarily the Ge are moving. This corresponds indeed to a so-called symmetric GeI₃ tetrahedron stretch mode as previous work interpreted it in terms of molecular mode analysis. Again, because of the opposite charges, there is a clear dipole character, which explains its strong IR absorption. Since the Raman A₁ tensor component b corresponds to z^2 and there is a large z displacement here, this also explains why this mode is strong in Raman. Similar analysis holds for the corresponding E-mode at slightly lower frequency. This one corresponds to the so-called asymmetric stretch mode, shown in Fig. 9e. One can see that in this mode the displacements are transverse to the C₃ rotation axis. It thus has strong infrared oscillator strength for x or y and strong $x^2 - y^2$ or xy like Raman intensity. In Fig. 9c we show the silent A₂ mode. This mode involves only motion of the I atoms in a complex rotational type pattern. In Fig. 9d finally, we show the mode E₃. In this mode the Ge as well as the I are moving but the I atoms have a rotational type motion. The dipole character is less clear and although this mode is indeed IR active, it has a small oscillator strength. Similar conclusions hold for the other weak intensity modes.

TABLE II. Comparison of measured Raman peak positions (in cm⁻¹) with our calculated phonon frequencies. The strength is indicated by vs,s,ls,m,w, which stand for very strong, strong, less strong, medium, weak.

Expt.1	Theory	Symmetry
CsGeI ₃		
151(s) ^a	156	E _{LO}
	161	A _{1LO}
105(vs) ^a	113	E _{TO}
172 ^b	159	$\frac{A_{1LO} + E_{LO}}{2}$
127 ^b	125	$\frac{A_{1TO} + E_{TO}}{2}$
CsGeBr ₃		
210(s) ^a , 209.79 ^c	200	A _{1LO}
	189	E _{LO}
160(ls) ^a , 159.88 ^c	165	A _{1TO}
139(vs) ^a , 140.31 ^c	136	E _{TO}
91(s) ^a , 93.99 ^c	83	A _{1TO+LO}
77(m) ^a , 78.50 ^c	67	E _{TO+LO}
49(w) ^a , 50.50 ^c	42	E _{TO+LO}
CsGeCl ₃		
290(s) ^a , 291.15 ^c	294	A _{1LO}
	273	E _{LO}
237(ls) ^a , 236.98 ^c	249	A _{1TO}
200(vs) ^a , 202.79 ^c	208	E _{TO}
145(m) ^a , 146.58 ^c	134	A _{1TO+LO}
120(w) ^a , 121.49 ^c	106	E _{TO+LO}
77(vw) ^a ,		
57(m) ^a , 58.50 ^c	59	E _{TO+LO}
	41	A _{1LO}
	37	E _{LO}

^a Tang *et al.*¹¹

^b Stoumpos *et al.*⁵

^c Lin *et al.*¹³

F. Born effective charges

In Table III we show the Born (or dynamical) effective charges. We can see that the sum $\sum_i Z_{i\alpha\beta}^* = 0$ with the sum over atoms for any given tensor element. This is required by the effective charge sum-rule. The Z*-tensor has non-zero off-diagonal elements for the halogen atoms X in the cell. The ones for X₂ and X₃ are obtained from those of X₁ by a three-fold rotation operation of the tensor. We can see that the Ge effective charge is even higher than 4 in the iodine case and decreases from iodine, to bromine to chlorine, reflecting the increased ionicity. This is in spite of the fact that nominally, the Ge is divalent in these compounds. The Cs and halogen effective charges follow a similar trend.

TABLE III. Born effective charges.

CsGeI ₃						
	xx	yy	zz	xy	xz	yz
Cs	1.6178	1.6178	1.6114			
Ge	4.2230	4.2230	3.0988			
I ₁	-0.1625	-3.7314	-1.5701			2.2970
I ₂	-2.8391	-1.0547	-1.5701	1.5454	1.9893	-1.1485
I ₃	-2.8391	-1.0547	-1.5701	-1.5454	-1.9893	-1.1485
CsGeBr ₃						
	xx	yy	zz	xy	xz	yz
Cs	1.5030	1.5030	1.4890			
Ge	3.5293	3.5293	2.9104			
Br ₁	-0.3518	-3.0030	-1.4664			1.7605
Br ₂	-2.3402	-1.0146	-1.4664	1.1480	1.5246	-0.8802
Br ₃	-2.3402	-1.0146	-1.4664	-1.1480	-1.5246	-0.8802
CsGeCl ₃						
	xx	yy	zz	xy	xz	yz
Cs	1.4086	1.4086	1.4106			
Ge	2.9609	2.9609	2.5137			
Cl ₁	-0.5290	-2.3841	-1.3081			1.2087
Cl ₂	-1.9203	-0.9927	-1.3081	0.8033	1.0468	-0.6044
Cl ₃	-1.9203	-0.9927	-1.3081	-0.8033	-1.0468	-0.6044

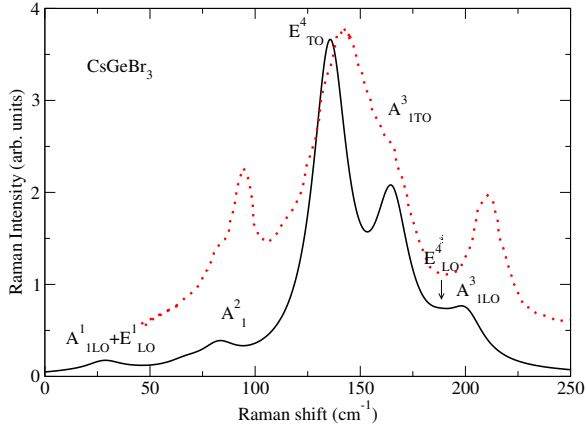


FIG. 7. (Color on-line) Direction and polarization averaged simulated Raman spectrum of CsGeBr₃ (black solid line) compared with the experimental data of Lin *et al.*¹³ (red dotted line). Calculated peaks are labeled by specific modes.

G. Dielectric constants.

In Table IV we give the high-frequency and static dielectric constant tensor elements. For a rhombohedral material, the dielectric tensor is diagonal and has $\varepsilon_{xx} = \varepsilon_{yy} \neq \varepsilon_{zz}$. We can see that the static dielectric

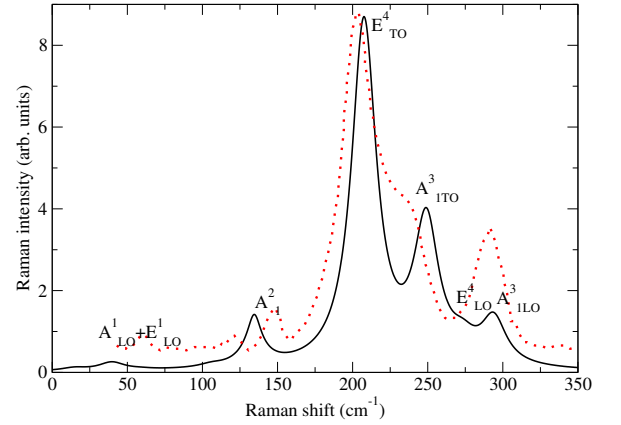


FIG. 8. (Color on-line) Direction and polarization averaged simulated Raman spectrum of CsGeCl₃ (black solid line) compared with the experimental data of Lin *et al.*¹³ (red dotted line). Calculated peaks are labeled by specific modes.

constants are very high. The ratios of $\varepsilon^0/\varepsilon^\infty$ range from about 4 to about 18. This corresponds to the high LO-TO splittings.

We can check the contribution of each mode to the

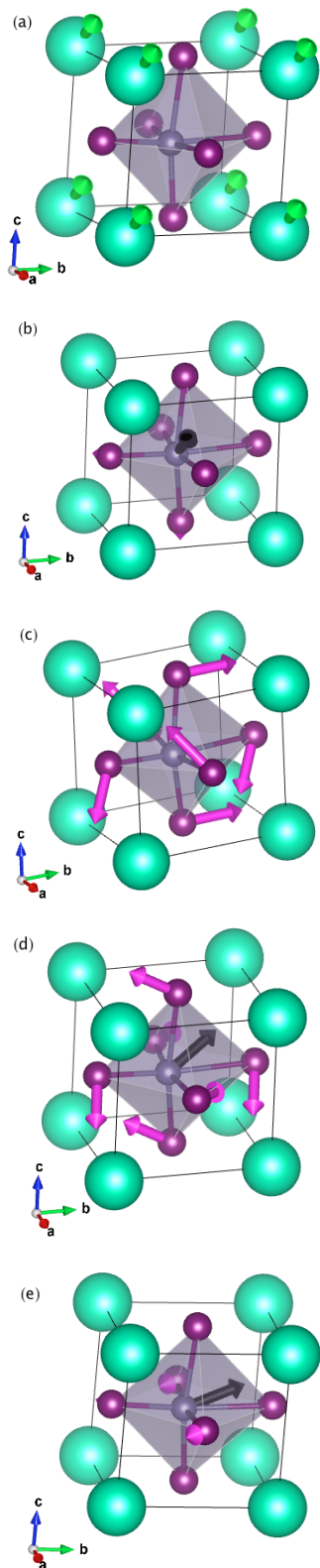


FIG. 9. (Color on-line) Mode patterns for selected modes in CsGeI_3 . The Ge is situated closest to the Cs in the left lower back corner of the figure, so that the 3-fold symmetry axis is the body diagonal from the back left to the top right. Large greenish spheres are Cs, the purple spheres are I and the grey one in the center of the octahedron is the Ge atom. Mode (a) is the lowest mode A_1 mode at 5.70 cm^{-1} , mode (b) corresponds to the highest A_1 mode at 137.21 cm^{-1} , mode (c) is the A_2 silent mode at 25.08 cm^{-1} and mode (d) is the third E mode at 50.64 cm^{-1} , mode (e) is the highest frequency E -mode at 113.56 cm^{-1} .

TABLE IV. Dielectric tensor components.

compound	ϵ_{xx}^∞	ϵ_{zz}^∞	ϵ_{xx}^0	ϵ_{zz}^0
CsGeI_3	9.63	9.98	33.76	181.89
CsGeBr_3	6.50	6.52	25.35	62.56
CsGeCl_3	4.30	4.13	41.98	52.13

TABLE V. Contribution of modes to the Lyddane-Sachs-Teller relation.

mode- i	$\left(\frac{\omega_{iLO}}{\omega_{iTO}}\right)^2$	$\prod_{j \leq i} \left(\frac{\omega_{jLO}}{\omega_{jTO}}\right)^2$	$\frac{\epsilon^0}{\epsilon^\infty}$
CsGeI_3			
A_1 -1	12.29	12.29	18.23
A_1 -2	1.07	13.15	
A_1 -3	1.39	18.23	
E -1	1.83	1.83	
E -2	1.01	1.85	3.50
E -3	1.01	1.87	
E -4	1.88	3.50	
CsGeBr_3			
A_1 -1	6.36	6.36	9.61
A_1 -2	1.02	6.52	
A_1 -3	1.47	9.61	
E -1	1.88	1.88	
E -2	1.05	1.98	3.90
E -3	1.02	2.01	
E -4	1.94	3.90	
CsGeCl_3			
A_1 -1	8.99	8.99	12.62
A_1 -2	1.01	9.06	
A_1 -3	1.39	12.62	
E -1	5.57	5.57	
E -2	1.01	5.61	9.75
E -3	1.002	5.62	
E -4	1.74	9.75	

Lyddane-Sachs-Teller (LST) relation,

$$\prod_i \left(\frac{\omega_{iLO}}{\omega_{iTO}}\right)^2 = \frac{\epsilon^0}{\epsilon^\infty} \quad (3)$$

where the product is over all A_1 modes for the zz component of ϵ and over all E -modes for the xx component of ϵ . Clearly, the lowest mode of A_1 symmetry makes the highest contribution because it has a large LO-TO splitting relative to the magnitude of the TO frequency, and hence a very large ratio. The unusually high LST contribution of this mode is due to the large displacement of the heavy Cs ion relative to the halogen ions which contributes a strong dipole even for a low frequency mode. For the E modes the lowest and highest IR mode make a comparable contribution to the LST factor.

H. Second-order nonlinear optics

Because these materials have been considered for nonlinear optical applications in the infrared, their second-

TABLE VI. Non-linear optical coefficients in pm/V.

	CsGeI ₃	CsGeBr ₃	CsGeCl ₃
d_{31}	-84.09	-22.03	-4.75
d_{22}	54.57	11.36	0.99
d_{33}	-64.93	-29.59	-9.76

TABLE VII. Inverse proportion of NLO coefficients to E_g^3 .

	E_g	$\frac{E_g(I)^3}{E_g(X)^3}$	$\frac{d_{31}(X)}{d_{31}(I)}$	$\frac{d_{22}(X)}{d_{22}(I)}$	$\frac{d_{33}(X)}{d_{33}(I)}$
CsGeI ₃	1.619	1	1	1	1
CsGeBr ₃	2.654	0.23	0.26	0.21	0.45
CsGeCl ₃	4.309	0.05	0.06	0.02	0.15

order non-linear optical coefficients are also of interest. For a material of point group $3m$ or C_{3v} , the nonlinear optical tensor is of the form:²⁵

$$\begin{bmatrix} 0 & 0 & 0 & 0 & d_{31} & -d_{22} \\ -d_{22} & d_{22} & 0 & d_{31} & 0 & 0 \\ d_{31} & d_{31} & d_{33} & 0 & 0 & 0 \end{bmatrix} \quad (4)$$

where the Kleinman symmetry is taken into account for low-frequencies. The calculated non-zero tensor elements are given in Table VI.

First, it is noticeable that all of these are quite large compared to $d_{36}(KDP) = 0.39$ pm/V of KH_2PO_4 or potassium dihydrogen phosphate, which is often used as a standard in NLO. Second, we note that the values decrease strongly from I to Br to Cl. This is in reverse order to the band gaps or ionicity. Second order NLO coefficients are indeed known to vary roughly as $1/E_g^3$. This relation is tested in Table VII, where we give the band gaps in column 1 and the ratios of $1/E_g^3$ relative to CsGeI₃ along with the corresponding ratios of the d_{13} , d_{22} and d_{33} . We can see that this scaling is pretty closely observed for d_{31} , somewhat less well for d_{22} and d_{33} . We here use the quasiparticle self-consistent *GW* band gaps calculated in Ref. 6. The nonlinear optical coefficients however are calculated at the LDA level.

The second harmonic generation of CsGeI₃ was studied by Stoumpos *et al.*⁵ for CsGeI₃ and other AGeI₃ with A being various organic ions. They also compare their results with CsGeBr₃ and CsGeCl₃ from Lin *et al.*^{13,26}. Keeping in mind that $\chi_{\text{eff}}^{(2)} = 2d_{\text{eff}}$ their values for d_{eff} are 64 pm/V, 12 pm/V and 0.6 pm/V for the I, Br, Cl case respectively. Unfortunately, they do not tell us which d_{eff} this corresponds to. It appears to be the one that is obtained under certain phase matching conditions but is not referred to specific crystalline directions because the measurements are on polycrystalline films. Nonetheless, these values are comparable with our d_{22} . Our values are thus at least consistent with experimental values in terms of order of magnitude.

From the point of view of non-linear optics, it is also of interest that the material is birefringent. The ordinary and extra-ordinary indices of refraction $n_o = \sqrt{\epsilon_{xx}^\infty}$,

$n_e = \sqrt{\epsilon_{zz}^\infty}$ and their difference $\Delta n = n_e - n_o$ are given in Table VIII. Interestingly, the I and Br case have positive while Cl has negative birefringence. Also, the absolute values of the birefringence of the I and Cl compounds are relatively high while that of Br is possibly too small to achieve phase-matching. Further detail on the indices of refraction as function of wavelength is required to evaluate in detail how suitable these materials are for NLO conversion phase matching.

TABLE VIII. Indices of refraction and birefringence.

	n_o	n_e	Δn
CsGeI ₃	3.104	3.159	0.055
CsGeBr ₃	2.550	2.553	0.002
CsGeCl ₃	2.075	2.033	-0.042

IV. CONCLUSIONS

A first-principles study was carried out for the zone-center phonon frequencies and associated spectra in CsGeX₃ compounds with X=I, Br, Cl. Fairly good agreement is obtained with the experimental data for the mode frequencies as extracted from Raman spectra. Various associated parameters were provided, including the oscillator strengths, the Raman tensor components, the dielectric constants and Born effective charges. The mode patterns and spectra were analyzed. Interestingly, there are two strongly IR active type of modes of each symmetry, one corresponding to motion of the Cs ions relative to the halogens at low frequency and one corresponding to the motion of the Ge ions relative to the halogens at high frequency. Only the latter is also strongly Raman active. The LO-TO splitting are sizable and lead to a very high ratio of the static to high-frequency dielectric constant components, especially for the A_1 symmetry or z component along the three-fold symmetry axis of the crystal. The non-linear optical coefficients were also calculated and show that these materials have competitively large second-harmonic conversion coefficients, especially for the lowest gap material CsGeI₃. They decrease rapidly from I to Br to Cl. Their values were found to be consistent with experimental values in literature for d_{eff} although the actual tensor components were not determined previously. We also find that CsGeI₃ has sizable positive birefringence, while CsGeCl₃ has sizable negative birefringence and CsGeBr₃ has only small birefringence in the static limit.

ACKNOWLEDGMENTS

This work was supported by the U.S. Department of Energy, Office of Science, Basic Energy Sciences under grant No. DE-SC0008933. The calculations made use of the High Performance Computing Resource in the Core

- * walter.lambrecht@case.edu
- ¹ M. M. Lee, J. Teuscher, T. Miyasaka, T. N. Murakami, and H. J. Snaith, *Science* **338**, 643 (2012).
 - ² M. Liu, M. B. Johnston, and H. J. Snaith, *Nature* **501**, 395 (2013).
 - ³ N.-G. Park, *Materials Today* **18**, 65 (2015).
 - ⁴ X. Y. Chin, D. Cortecchia, J. Yin, A. Bruno, and C. Soci, *Nat Commun* **6**, 7383 (2015).
 - ⁵ C. C. Stoumpos, L. Frazer, D. J. Clark, Y. S. Kim, S. H. Rhim, A. J. Freeman, J. B. Ketterson, J. I. Jang, and M. G. Kanatzidis, *Journal of the American Chemical Society* **137**, 6804 (2015), pMID: 25950197, <http://dx.doi.org/10.1021/jacs.5b01025>.
 - ⁶ L.-y. Huang and W. R. L. Lambrecht, *Phys. Rev. B* **93**, 195211 (2016).
 - ⁷ A. M. Glazer, *Acta Crystallographica Section B* **28**, 3384 (1972).
 - ⁸ L.-y. Huang and W. R. L. Lambrecht, *Phys. Rev. B* **90**, 195201 (2014).
 - ⁹ I. Chung, J.-H. Song, J. Im, J. Androulakis, C. D. Malliakas, H. Li, A. J. Freeman, J. T. Kenney, and M. G. Kanatzidis, *Journal of the American Chemical Society* **134**, 8579 (2012), <http://pubs.acs.org/doi/pdf/10.1021/ja301539s>.
 - ¹⁰ G. Thiele, H. W. Rotter, and K. D. Schmidt, *Z. anorg. allg. Chem.* **545**, 148 (1987).
 - ¹¹ L.-C. Tang, C.-S. Chang, L.-C. Tang, and J. Y. Huang, *Journal of Physics: Condensed Matter* **12**, 9129 (2000).
 - ¹² L. C. Tang, J. Y. Huang, C. S. Chang, M. H. Lee, and L. Q. Liu, *Journal of Physics: Condensed Matter* **17**, 7275 (2005).
 - ¹³ Z.-G. Lin, L.-C. Tang, and C.-P. Chou, *Inorganic Chemistry* **47**, 2362 (2008), pMID: 18318478, <http://dx.doi.org/10.1021/ic7011777>.
 - ¹⁴ X. Gonze, *Phys. Rev. B* **55**, 10337 (1997).
 - ¹⁵ X. Gonze and C. Lee, *Phys. Rev. B* **55**, 10355 (1997).
 - ¹⁶ S. Baroni, P. Giannozzi, and A. Testa, *Phys. Rev. Lett.* **58**, 1861 (1987).
 - ¹⁷ P. Giannozzi, S. de Gironcoli, P. Pavone, and S. Baroni, *Phys. Rev. B* **43**, 7231 (1991).
 - ¹⁸ X. Gonze, J. M. Beuken, R. Caracas, F. Detraux, M. Fuchs, G. M. Rignanese, M. Sindic, L. and Verstraete, G. Zerah, and F. Jollet, *Computational Materials Science* **25,3**, 478 (2002/11).
 - ¹⁹ C. Hartwigsen, S. Goedecker, and J. Hutter, *Phys. Rev. B* **58**, 3641 (1998).
 - ²⁰ J. P. Perdew and Y. Wang, *Phys. Rev. B* **45**, 13244 (1992).
 - ²¹ D. M. Ceperley and B. J. Alder, *Phys. Rev. Lett.* **45**, 566 (1980).
 - ²² S. Goedecker, M. Teter, and J. Hutter, *Phys. Rev. B* **54**, 1703 (1996).
 - ²³ M. Veithen, X. Gonze, and P. Ghosez, *Phys. Rev. B* **71**, 125107 (2005).
 - ²⁴ S. P. S. Porto, J. A. Giordmaine, and T. C. Damen, *Phys. Rev.* **147**, 608 (1966).
 - ²⁵ R. W. Boyd, *Nonlinear Optics* (Academic Press, Boston, 1992).
 - ²⁶ Z.-G. Lin, L.-C. Tang, and C.-P. Chou, *Journal of Physics: Condensed Matter* **19**, 476209 (2007).